Materials and Design 67 (2015) 50–63

Contents lists available at ScienceDirect

Materials and Design

journal homepage: www.elsevier.com/locate/matdes

Effect of boron and carbon addition on microstructure and mechanical properties of metastable beta titanium alloys

Ravinaik Banoth [a], Rajdeep Sarkar [b], Amit Bhattacharjee [b,*], T.K. Nandy [b], G.V.S. Nageswara Rao [a]

[a] Department of Metallurgical and Materials Engineering, National Institute of Technology, Warangal 506004, India
[b] Defence Metallurgical Research Laboratory, P.O. Kanchanbagh, Hyderabad 500058, India

ARTICLE INFO

Article history:
Received 14 August 2014
Accepted 3 November 2014
Available online 10 November 2014

Keywords:
β-Titanium alloys
Boron and carbon
Solution treatment
Ageing
Electron microscopy
Tensile testing

ABSTRACT

Effect of boron and carbon on microstructure and mechanical properties of β titanium alloys Ti–15V–3Cr–3Mo–3Sn, Ti–10V–2Fe–3Al, and Ti–5V–5Mo–5Al–3Cr has been studied in detail. The addition of boron and carbon results in refinement of β grain size and α-precipitates during ageing. While the hardness and tensile strength increase with the addition of boron and carbon, the elongation to failure deteriorates. The increase in strength is attributed to a synergistic effect of grain refinement and load sharing by TiB and TiC particles; whereas decrease in elongation is due to the brittleness of these hard particles. Ageing results in increase in strength and decrease in elongation as compared to solution treatment condition. In this case, the effect of boron and carbon is marginal. Further enhancement in the properties can be achieved by fine tuning heat treatment parameters. Multiple slopes are observed in log–log plots of true stress–true strain thereby implying different deformation mechanisms over a large range of plastic deformation.

1. Introduction

Beta titanium alloys have been extensively used for aerospace structural applications [1,2]. It is primarily because of three attributes [3]: (1) relatively lower density as compared to steels and nickel base super alloy, (2) reasonable balance of modulus, strength, ductility and fracture toughness, and (3) excellent corrosion resistance. Additionally, the alloy can be heat treated to obtain a range of mechanical properties depending upon the application [4]. In a very recent study carried out by Srinivasu and co-workers [5], the effect of thermo-mechanical processing on tensile and fracture toughness of a high strength beta titanium alloy has been clearly shown.

Some of the applications of β-titanium alloys include landing gears, slat and flap tracks, springs, brackets and so on [1]. Since the use of β-titanium alloys results inconsiderable weight saving and, therefore increased fuel efficiency of an aircraft, there is a continuous drive towards increasing use of these alloys. This is possible by improving the mechanical properties (especially the strength and fracture toughness) of these alloys. The alloys are used at room temperature as well as moderately high temperatures. Therefore, any attempt to improve the properties of the alloy should address both low and high temperature (25–500 °C) properties. In recent times, additions of boron and carbon in beta titanium alloys have been attempted with beneficial effects. Small addition of carbon leads to significant refinement in the microstructure of an aged β-titanium alloy [6]. Similarly fine microstructure with boron addition has been obtained in pure titanium [7] and titanium alloys such as Ti–6Al–4V and Ti–6Al–2Sn–4Zr–2Mo [8]. Grain boundary pining effect of TiB whiskers has also been shown by Cherukuri and co-workers [9]. A study on synergistic effect of boron and carbon on Ti–15V–3Al–3Sn–3Cr has shown similar results [10]. While the addition of boron results in substantial refinement in beta/prior beta grain size, carbon addition is associated with refinement in the aged microstructure. Additionally these additions also lead to nucleation of undeformable particles such as TiB and TiC. Thus, refinement in microstructure and the presence of undeformable particles lead to strengthening of these alloys. Extensive work carried out on the effect of boron addition in near alpha and alpha–beta alloys has clearly established the beneficial effect of boron on both room and high temperature properties [12]. Ranganath and Mishra [13] also showed beneficial effects of B_4C addition in Ti–6Al–4V alloy.

Therefore in the present investigation, the effect of boron and carbon addition in three beta titanium alloys namely Ti–15V–3Cr–3Al–3Sn (Ti-15333), Ti–10V–2Fe–3Al (Ti-1023) and Ti–5V–5Mo–5Al–3Cr (Ti-5553) has been studied. The alloys with B and

* Corresponding author. Tel.: +91 4024586601.
E-mail address: amitb@dmrl.drdo.in (A. Bhattacharjee).

http://dx.doi.org/10.1016/j.matdes.2014.11.004
0261-3069/

Table 1
Chemical composition of the selected titanium alloys (wt.%).

Titanium alloy	V	Cr	Al	Fe	Mo	Sn	B	C	N	O	Ti
Ti–15V–3Cr–3Al–3Sn (Ti-15333)	14.2	2.7	3.2	–	–	2.2	–	–	0.004	0.102	Bal.
Ti–15V–3Cr–3Al–3Sn–0.1B–0.1C (Ti-15333BC)	14.9	3.1	3.1	–	–	2.3	0.07	0.11	0.005	0.12	Bal.
Ti–10V–2Fe–3Al (Ti-1023)	9.50	–	3.1	2.3	–	–	–	–	0.003	0.110	Bal.
Ti–10V–2Fe–3Al–0.1B–0.1C (Ti-1023BC)	9.70	–	3.2	1.8	–	–	0.08	0.11	0.006	0.13	Bal.
Ti–5V–5Al–5Mo–3Cr (Ti-5553)	4.00	2.4	3.9	–	3.5	–	–	–	0.006	0.105	Bal.
Ti–5V–5Al–5Mo–3Cr–0.1B–0.1C (Ti-5553BC)	5.00	2.8	4.6	–	4.4	–	0.07	0.11	0.007	0.12	Bal.

Fig. 1. As forged pancakes (diameter: 130 mm, thickness: 7 mm) of some selected titanium alloys.

C designated as Ti-15333BC, Ti-1023BC and Ti-5553BC along with base line compositions (Table 1) have been investigated. While Ti-15333 and Ti-1023 are earlier generation alloys used for a variety of aerospace applications [14], Ti-5553 is a relatively recent alloy mainly developed for landing gear applications [15]. The effect of these additions on microstructure of solution treatment and solution treated plus aged conditions have been studied first. This is followed by the evaluation of hardness and tensile properties in single phase beta and aged beta structure (comprising fine alpha in a beta matrix). Structure–property correlation has been carried out to understand: (1) the effect of ageing on mechanical properties in a given composition and (2) the effect of boron and carbon addition on microstructure and properties of the alloys in both solution treatment and solution treatment plus aged conditions.

2. Experimental procedure

The alloys were melted by non-consumable vacuum arc melting to obtain 600 g pancakes. The melting was repeated four times to get a homogenous pancake. While V was added as V-Al master alloy, elements such as Al, Sn, Cr, C and B were added in pure elemental form. The alloys without boron and carbon were also melted to generate base line microstructures and mechanical property data. Chemical analysis of Al, Sn, Cr, V and B was carried out using Inductively Coupled Plasma-Optical Emission Spectroscope (ICP OES) instrument and O, N, and C were analysed using Leco analyser. Chemical analysis results are shown in Table 1. The alloys were hot forged to about 7 mm thickness from 10 mm initial thickness thereby giving an overall deformation of 30%. Fig. 1 shows as-forged pancakes of some alloys.

The hot forged alloys were given two different heat-treatments: (1) solution treatment (ST) for 1 h followed by water quenching and (2) solution treatment plus aging (STA) at 500 °C for 8 h followed by air-cooling. This was done to generate two different microstructures, namely, single-phase β and aged β (containing fine α in retained β matrix) respectively. The details of forging and heat treatment are given in Table 2.

Standard metallographic polishing techniques were employed for microstructural observation using optical and scanning electron microscope (SEM) and finally etching was carried out with Kroll's reagent (2 ml of HF, 4 ml of HNO_3, 94 ml of distilled water). Etched samples were examined under optical and SEM. For transmission electron microscopy, specimens were prepared by mechanically polishing the discs of 3 mm dia up to 100 μm and then electro-polishing in twin jet electro polisher (FISCHIONE Instrument, Model: 110). Electro-polishing was done using 5% H_2SO_4 solution in methanol as electrolyte at 223 K. During polishing, the voltage was maintained at 20 V. A Tecnai G^2 20 T Transmission Electron Microscope (TEM) was used for the examination of the foils.

Hardness of all selected materials, both in solution treated and solution treated plus aged condition, was measured by using Shimadzu microhardness tester (model HMV 2000), applying a load of 500 g with a dwell time of 15 s. Room temperature tensile tests were performed on flat tensile specimens. During tensile specimen preparation, 1 mm layer was machined out from both top and bottom surfaces in order to remove the oxide layer formed during forging and heat treatment. A screw driven Instron machine (5500R) was used for the tests at a strain rate of 10^3 s^1. Engineering stress–strain data were extracted from the load–elongation curves recorded during the tests. The tensile tests were carried out according to ASTM: E8M-142 in flat type fixer digital control INSTRON 5500R test system in order to obtain the stress-strain curves. Fracture surfaces of the failed specimens were observed using scanning electron microscope.

3. Results

3.1. Chemical composition and microstructure

Optical microstructures of the alloys in solution treatment conditions are shown in Fig. 2. Equiaxed microstructure is seen in all

Table 2
Beta-transus temperature, forging temperature and heat treatment details of titanium alloys investigated.

Titanium alloy	Ti-15333	Ti-15333BC	Ti-1023	Ti-1023BC	Ti-5553	Ti-5553BC
Forging temperature (°C)	900	900	950	950	1000	1000
Solution treatment	810 °C/1 h/WQ		850 °C/1 h/WQ		900 °C/1 h/WQ	
Ageing	500 °C/8 h/AC					

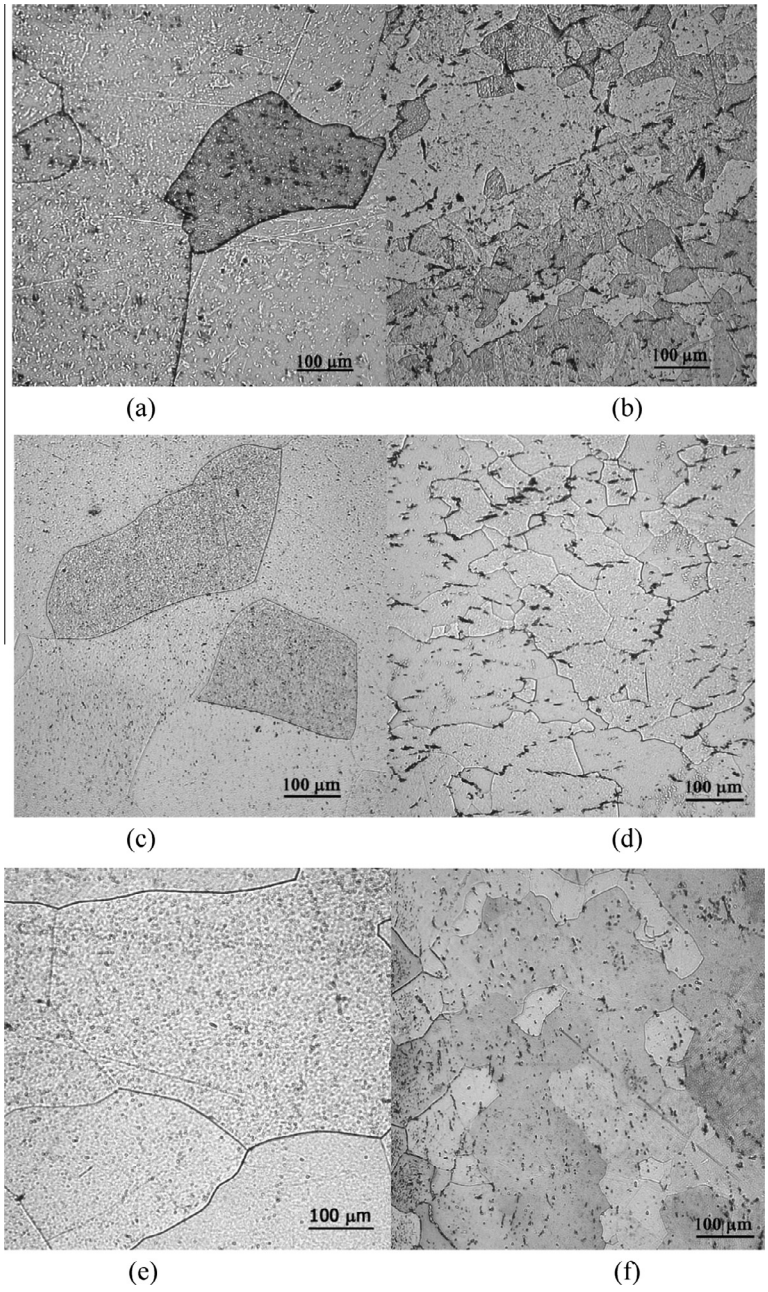

Fig. 2. Optical microstructures of solution treated alloys. (a) Ti-15333, (b) Ti-15333BC, (c) Ti-1023, (d) Ti-1023BC, (e) Ti-5553 and (f) Ti-5553BC. Refinement in grain size of the alloys with boron and carbon is clearly seen.

cases. In some cases, especially in the alloys without boron and carbon, the grains are non-uniform in size. As compared to the compositions without boron and carbon, the alloys containing boron and carbon show significantly refined grains and also the grain size distribution appears to be more uniform. This is clearly brought out in Table 3, which shows the grain size of all alloys with corresponding standard deviation.

Optical micrographs of the aged specimens are shown in Fig. 3. The structure is too fine to be resolved at optical level (magnifications ranging from 50 to 500×). Scanning secondary electron images recorded at higher magnification for the alloy Ti-5553 in solution heat treatment plus aged condition is shown in Fig. 4. It is clearly seen that the alloy containing boron and carbon shows higher volume fraction of α precipitates as compared to the one without boron and carbon. Also, in this case, the distribution of α

Table 3
Grain size of the alloys in different heat treatment conditions.

Titanium alloy	Heat treatment condition	Grain size, μm
Ti-15333	ST	225 ± 51
Ti-15333BC	ST	52 ± 12
Ti-1023	ST	530 ± 51
Ti-1023BC	ST	38 ± 12
Ti-5553	ST	295 ± 50
Ti-5553BC	ST	45 ± 13
Ti-15333	STA	210 ± 31
Ti-15333BC	STA	44 ± 18
Ti-1023	STA	483 ± 51
Ti-1023BC	STA	56 ± 12
Ti-5553	STA	308 ± 51
Ti-5553BC	STA	42 ± 13

ST: solution treated; STA: solution treated plus aged.

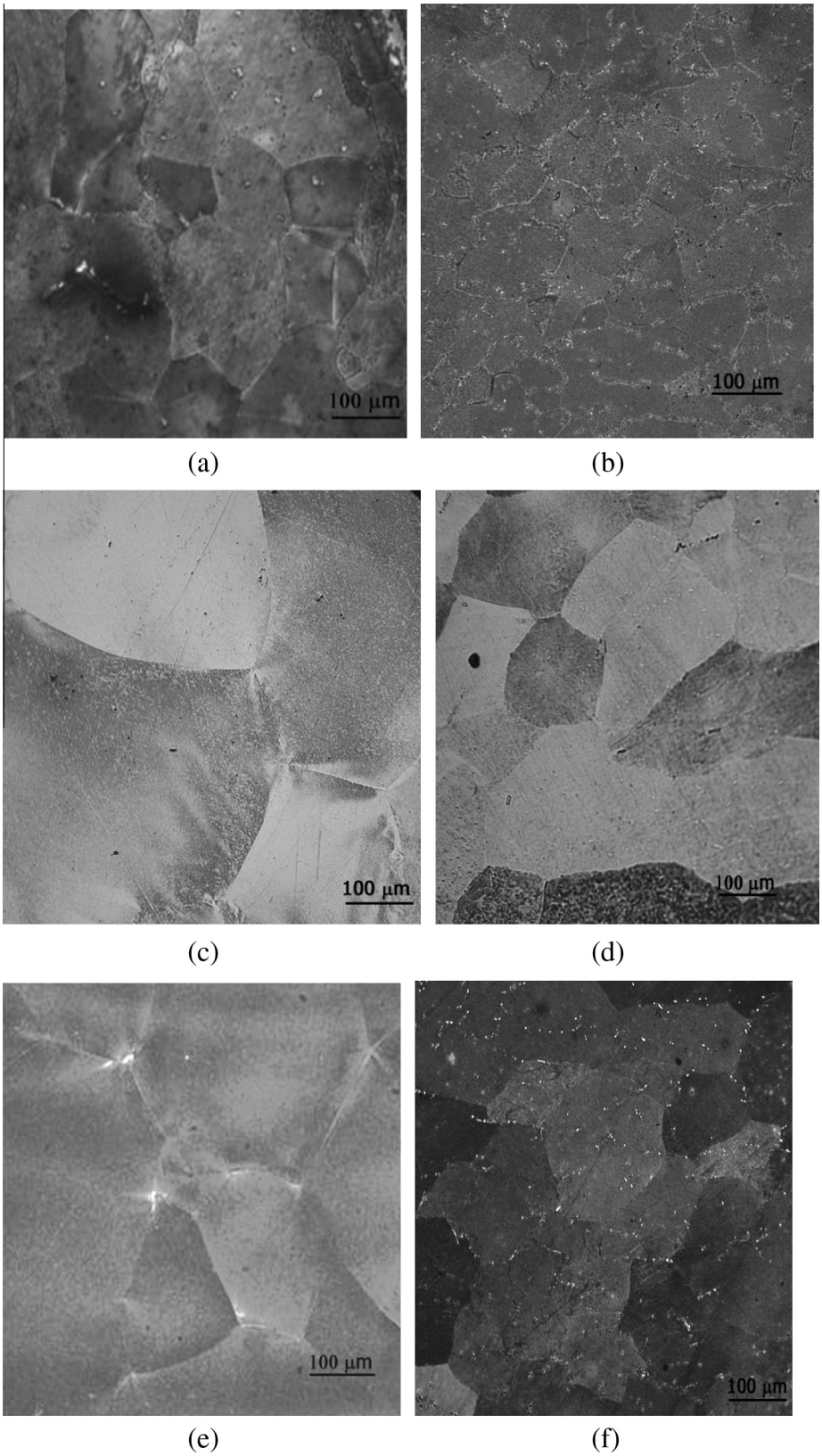

Fig. 3. Optical microstructures of solution treated plus aged alloys. (a) Ti-15333, (b) Ti-15333BC, (c) Ti-1023, (d) Ti-1023BC, (e) Ti-5553 and (f) Ti-5553BC. Also show refinement in prior beta grains with boron and carbon addition.

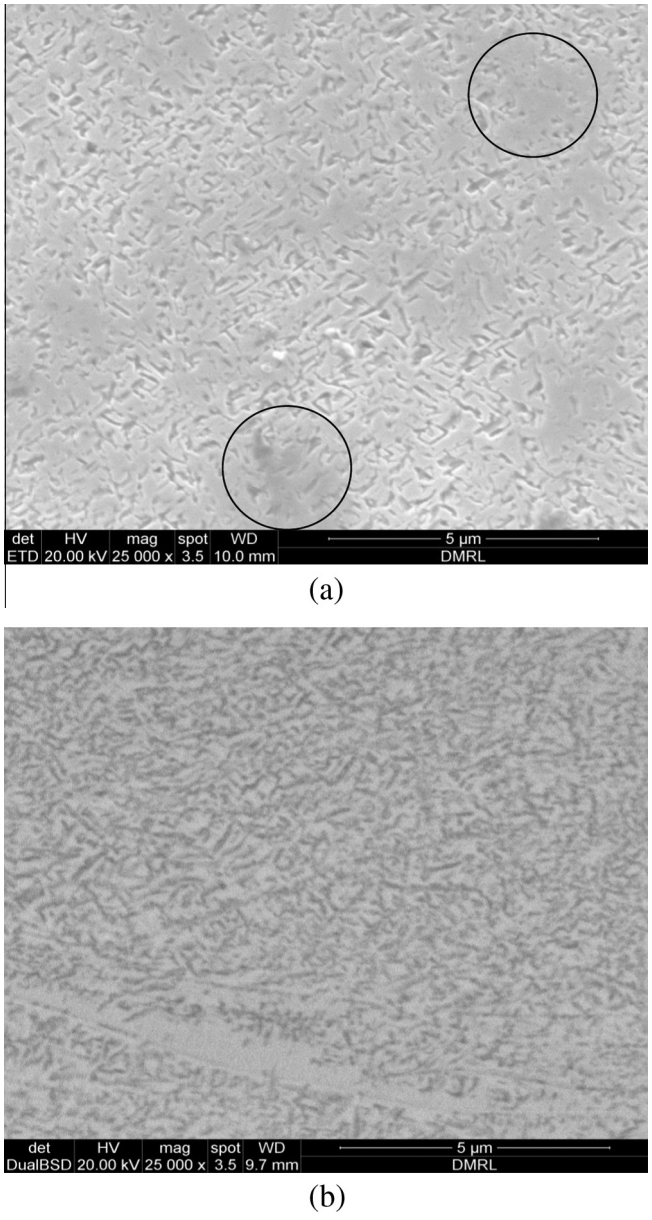

Fig. 4. Distribution of alpha particles in Ti-5553 alloy, (a) without and (b) with boron and carbon, in solution treatment plus aged condition. Patches of precipitate free zone (shown by circles) can be seen in the alloy without boron and carbon.

precipitates is finer and more uniform in the alloy with boron and carbon. Regions of precipitate free zone observed in the base alloy are absent in the alloy with boron and carbon. A bright field image of an aged microstructure of Ti-5553BC alloy with a composite diffraction pattern is shown in Fig. 5. Two different variants of alpha that are almost perpendicular to each other are seen.

Higher magnification images of Ti-15333BC and Ti-1023BC alloys in solution treatment plus aged condition were recorded to reveal the distribution of carbide and boride. This is shown in Fig. 6. The particles that show darker contrast in back scattered mode mostly decorate the grain boundaries. The morphology of these particles is clearly seen in Fig. 7. While boride particles are plate like, the carbide particles are round. Precipitation of carbide over boride particles is also noticed (Fig. 7).

Fig. 8a shows a bright field TEM image of TiC particle in the alloy Ti-5553BC. Corresponding selected area diffraction pattern confirming the presence of this phase is shown in Fig. 8b. TiB particle in the same alloy and its diffraction pattern are shown in Fig. 8c and d respectively. Heavily faulted structure is seen in the TiB particle.

3.2. Mechanical properties

Table 4 and Fig. 9 show hardness values of different alloys in solution treatment and solution treatment plus aged condition. It can be clearly seen that for the same heat treatment condition, the alloys containing boron and carbon show higher hardness than the base alloys without boron and carbon except Ti-1023BC in aged condition where the alloy containing boron and carbon shows a mild drop in the hardness value. The hardness increases significantly after ageing. This increase is more in Ti-5553 alloy.

Figs. 10 and 11 show engineering stress–strain curves of alloys Ti-15333 and Ti-5553 with and without boron and carbon addition. In solution treated condition, the stress–strain curve shows four distinct regions: (1) linear elastic region, (2) stage I, where the stress increases rapidly with increasing plastic strain, (3) stage II, where the increase in stress is gradual or in some cases, it decreases with increasing strain, and (4) stage III, where the stress drop is rapid pointing towards necking. These regimes are clearly seen in Ti-5553 (Fig. 11a). Ti-15333, on the other hand, does not show a pronounced necking behaviour. In fact, Ti-15333 shows decreasing engineering stress with increasing strain.

The alloys with boron and carbon show a varied behaviour depending upon the system. In Ti-15333 alloy system, the stress values increase with strain (Fig. 10a). This is in contrast to the base alloy (without boron and carbon) where the stress value decreases with increasing strain. On the other hand, both Ti-5553 and Ti-5553BC show decreasing stress with increasing strain prior to necking (Fig. 11a).

The tensile properties of the alloy (average of four data points) in solution heat treatment condition are listed in Table 5a. Yield, ultimate tensile and fracture stress values are higher in boron–carbon containing alloys as composed to their baseline counter parts without boron and carbon. However, the elongation-to-failure values are significantly lower in boron–carbon containing alloy. It drops by almost one-third in all cases.

The tensile curves of Ti-15333 and Ti-5553 in aged condition are shown in Figs. 10b and 11b respectively. It is very clear that the strength values go up and percent elongation decreases drastically as compared to solution treatment condition. In case of boron–carbon alloys, while the strength values increase further,

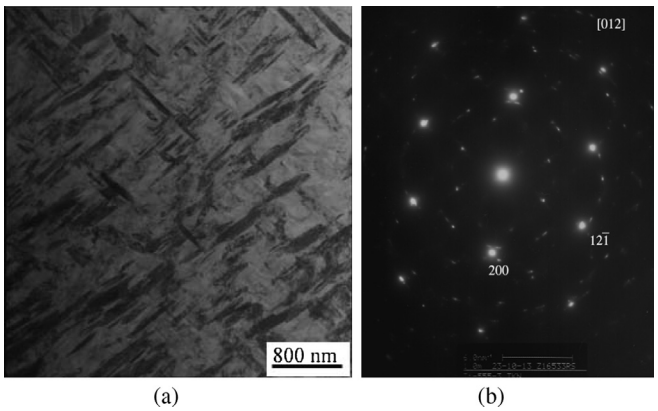

Fig. 5. (a) Aged structure of Ti-5553BC alloy comprising retained beta and alpha and (b) its composite diffraction pattern.

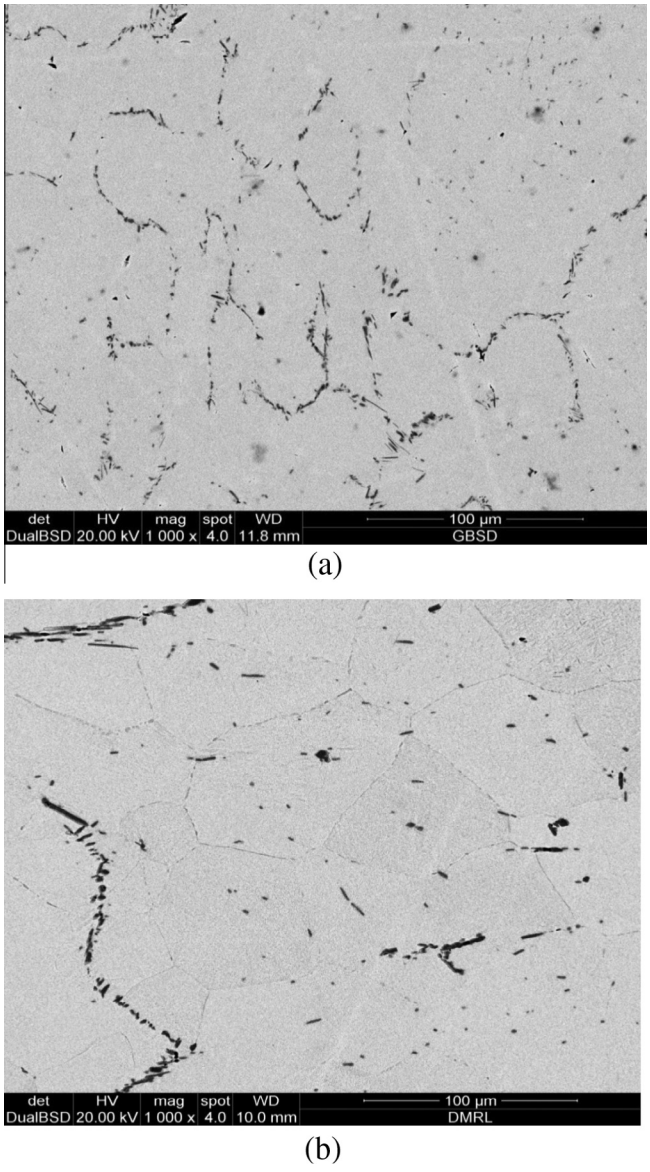

Fig. 6. High magnification SEM images of (a) Ti-15333BC, (b) Ti-1023BC in STA condition, showing distribution and morphology of borides (plate like particles) and carbides (round particles).

elongation values decrease. Only Ti-15333 and Ti-5553 show elongation values exceeding 1%. The properties are listed in Table 5b.

The fractographs of failed tensile specimen are shown in Figs. 12–15. While low magnification pictures are shown in Figs. 12 and 13, high magnification images are shown in Figs. 14 and 15. In the solution heat treatment condition, while the base alloy shows coarse features, the alloys with boron and carbon show finer features. Ductile dimples are seen in all three base alloys whereas in the alloys with boron and carbon, the occurrence of dimples is less. One can see featureless regions in boron-carbon alloys. In aged specimen, especially at lower magnification, mixed mode failure comprising intergranular plus transgranular failure is seen. Again in these cases, boron–carbon containing alloys show finer features as compared to the base alloy. The alloys with boron and carbon show transgranular feature as compared to mixed failure in the base alloys. However at higher magnification, while well developed dimple failure pointing towards micro plasticity is seen in the base alloys, the one with boron and carbon either show very fine dimples or flat features.

4. Discussion

4.1. Microstructure

Microstructure of titanium alloys with the addition of boron and carbon has been studied in considerable detail. Significant reduction in grain size with boron addition has been observed in pure titanium [7], near alpha alloys such as Ti–6Al–2Sn–4Zr–2Mo [8], Timetal 685 [16] and alpha–beta alloy Ti–6Al–4V [8,17]. The refining action of boron has been ascribed to constitutional supercooling that occurs in boron containing alloys. As the dendrite nucleates from the molten pool, it rejects boron rich liquid ahead of the dendrite tip that restricts the growth of dendrite and facilitates fresh nucleation leading to a finer microstructure. Similar observation has also been reported in beta titanium alloys such as Ti-21S and Ti-5553 [9,11]. In all these cases, refinement has been observed in as cast condition. Recently, Sarkar et al. [10] also showed refinement in microstructure in Ti-15333 alloy with boron and carbon. In this case refinement was observed in rolled plus heat treated condition. While the base alloy showed a grain size of 211 µm, the alloys containing boron and carbon showed grain size of 135 and 72 µm respectively. The refinement in the structure was attributed to the pinning effects of boride and carbide. The presence of carbide resulted in higher refinement possibly because of their finer precipitate size and distribution. While in their study the degree of refinement was by a factor of 2–3; in the present case, the extent of refinement is by a factor of 4–8. Thus, it appears that the combined influence of boron and carbon is more than their individual effects. This may be due to the higher volume fraction of TiB and TiC combined. An example of TiC and TiB populating the grain boundary is shown in Fig. 7.

The refinement of aged alpha observed in the present study is consistent with the observations of Wu and co-workers [18] and Sarkar and co-workers [10,19]. Additionally they also report more homogenous distribution of alpha in the carbon containing alloy. It has been proposed by Wu and co-workers [18] that carbon present in the solid solution of beta forms complexes with interstitials and vacancies. These act as nucleation sites for the aged alpha thereby making the structure more refined and homogenous. While the

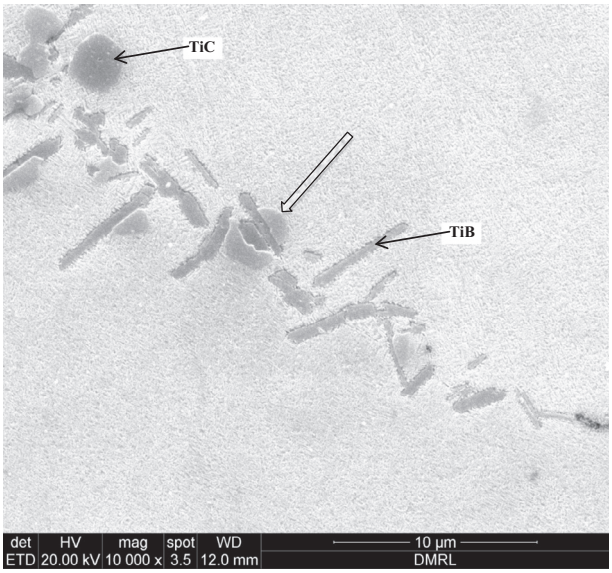

Fig. 7. Distribution of borides and carbides in the vicinity of grain boundary in Ti-5553BC (solution treated plus aged). Arrow shows precipitation of carbide over boride particles.

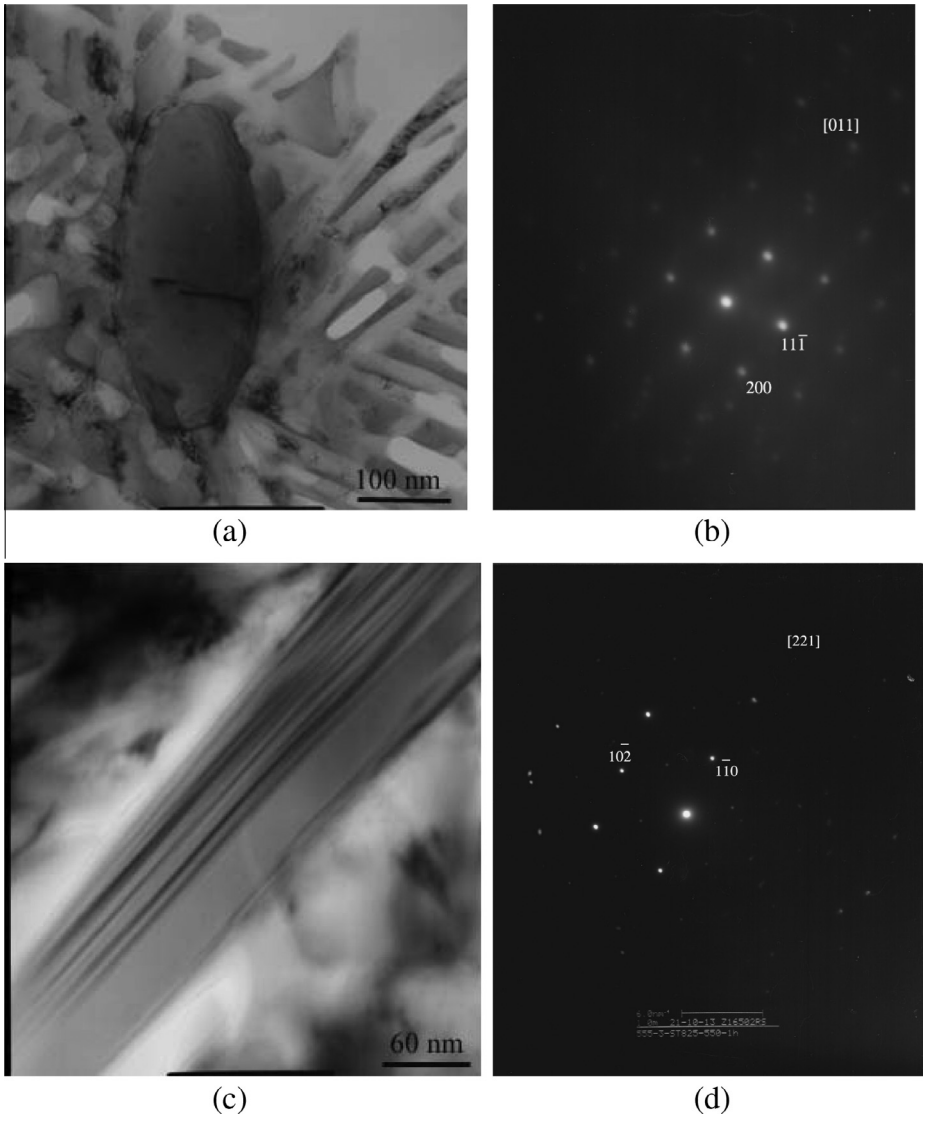

Fig. 8. Bright field images of (a) TiC, (b) its corresponding SADP, (c) TiB particles (showing a faulted structure), and (d) its corresponding SADP, in Ti-5553BC.

Table 4
Hardness values of the selected titanium alloys in different heat treatment conditions.

Titanium alloy	Heat treatment condition	Microhardness, $HV_{0.5}$ Average value
Ti-15333	ST	285.8
	STA	416.8
Ti-15333BC	ST	360.1
	STA	480.9
Ti-1023	ST	323.9
	STA	460.1
Ti-1023BC	ST	342.7
	STA	453.1
Ti-5553	ST	299.2
	STA	508.4
Ti-5553BC	ST	308.1
	STA	531.8

ST: solution treated; STA: solution treated plus aged.

morphology of boride is needle like, that of carbide is spherical. This is also in line with those reported by Sarkar and co-workers [10] and Chandravanshi and coworkers [16]. The faulted structure in TiB has been also reported by the above mentioned researchers.

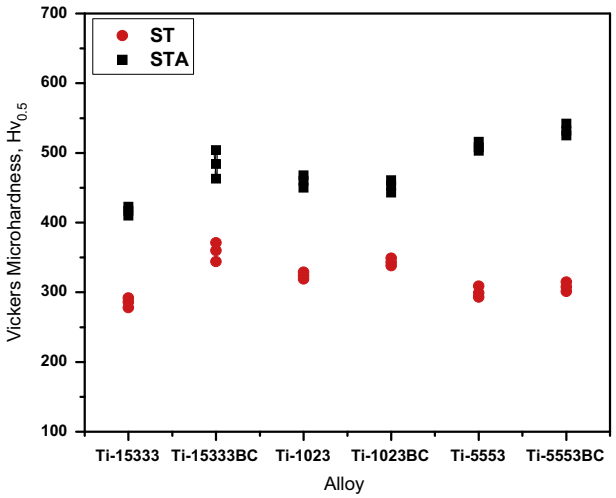

Fig. 9. Microhardness of solution treated and solution treated plus aged alloys. Increase in hardness with the addition of boron and carbon and also ageing is clearly seen.

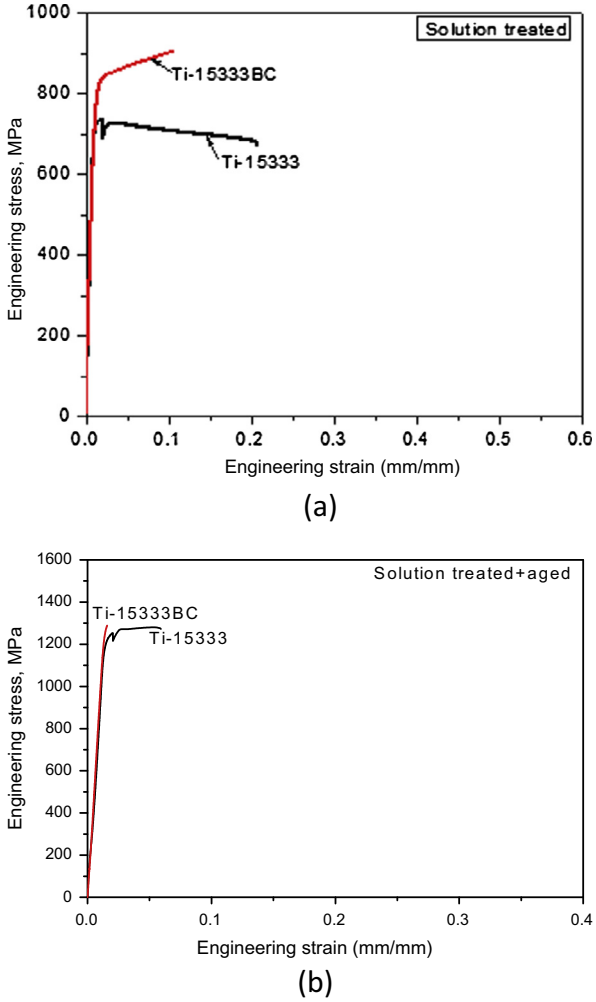

Fig. 10. Engineering stress–strain curves of Ti-15333 alloy with and without boron and carbon in (a) solution treated, and (b) solution treated plus aged.

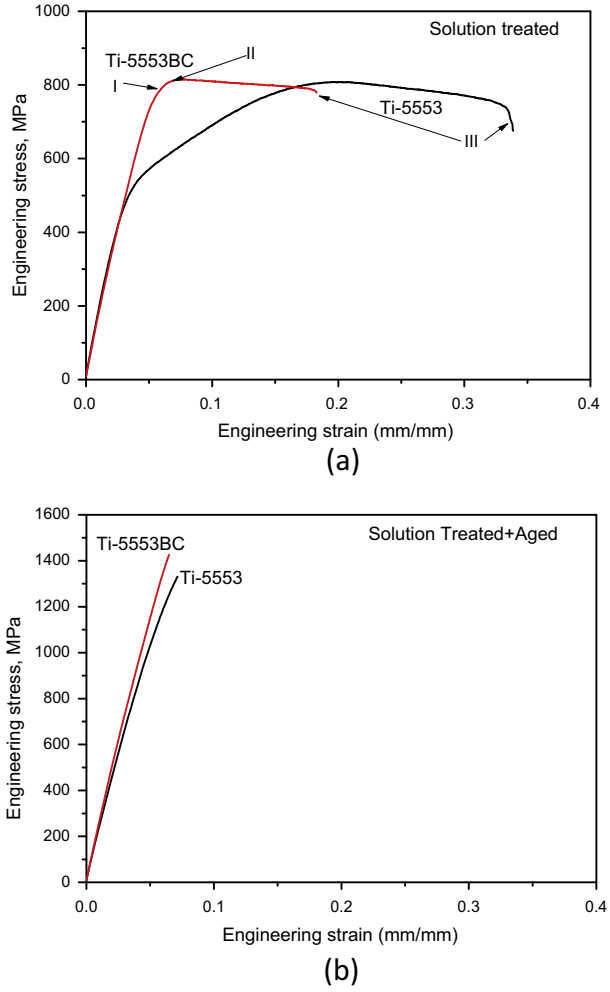

Fig. 11. Engineering stress–strain curves of Ti-5553 alloy with and without boron and carbon in (a) solution treated and (b) solution treated plus aged.

Thus, the addition of boron and carbon results in considerable refinement of both prior beta grain size and aged alpha precipitates. Additionally, the grain size distribution of beta is more uniform. This is especially important because obtaining uniform prior grain size in β titanium alloys is difficult since the processing window for realising such a microstructure is very narrow.

4.2. Mechanical properties

The increase in hardness in boron–carbon containing alloys as compared to the base alloys in all three cases in solution treatment condition is possibly due to two factors: (1) refinement in grain size leading to Hall–Petch [20,21] effect and (2) hard and undeformable particles of boride and carbide. An extensive amount of work has been done to explain strengthening of alloys in the presence of undeformable particles. The model developed by Boehlert and co-workers [22] based on deformation of metal–matrix composite containing aligned plus fragmented whiskers has been used. While Chandravanshi and co-workers [23] have used it to explain strengthening in near alpha titanium alloy, Sarkar and co-workers [10] have applied it to beta titanium alloy. Based on their work, it is proposed that the strengthening in boron-carbon containing alloy is due to a synergistic effect of grain refinement and the presence of undeformable particles.

Table 5
Mechanical properties of titanium alloys investigated.

Titanium alloy	Yield stress, MPa	Ultimate tensile strength, MPa	Fracture stress, MPa	% El
(a) in solution treated (ST) condition				
Ti-15333	701	728	598	20.2
Ti-15333BC	769	834	815	9
Ti-1023	576	812	804	45.7
Ti-1023BC	695	829	818	15.1
Ti-5553	461	794	572	32.1
Ti-5553BC	759	842	807	12.2
(b) in solution treated plus aged (STA) condition				
Ti-15333	1179	1240	1287	4.3
Ti-15333BC	1278	1277	1277	0.3
Ti-1023	932	1306	1306	0.73
Ti-1023BC	1305	1385	1358	0.98
Ti-5553	1107	1267	1265	1.2
Ti-5553BC	1400	1463	1463	0.5

Substantial jump in hardness due to ageing is attributed to precipitation of alpha in β matrix. This results in lot of α–β interfaces that provide obstacles to dislocation motion [4]. The addition of boron plus carbon leads to only marginal strengthening. In fact in Ti-1023, there is a minor drop in the hardness in the boron–carbon containing alloy. Since the hardness jump due to ageing is substantially high, the mild strengthening effect brought about by

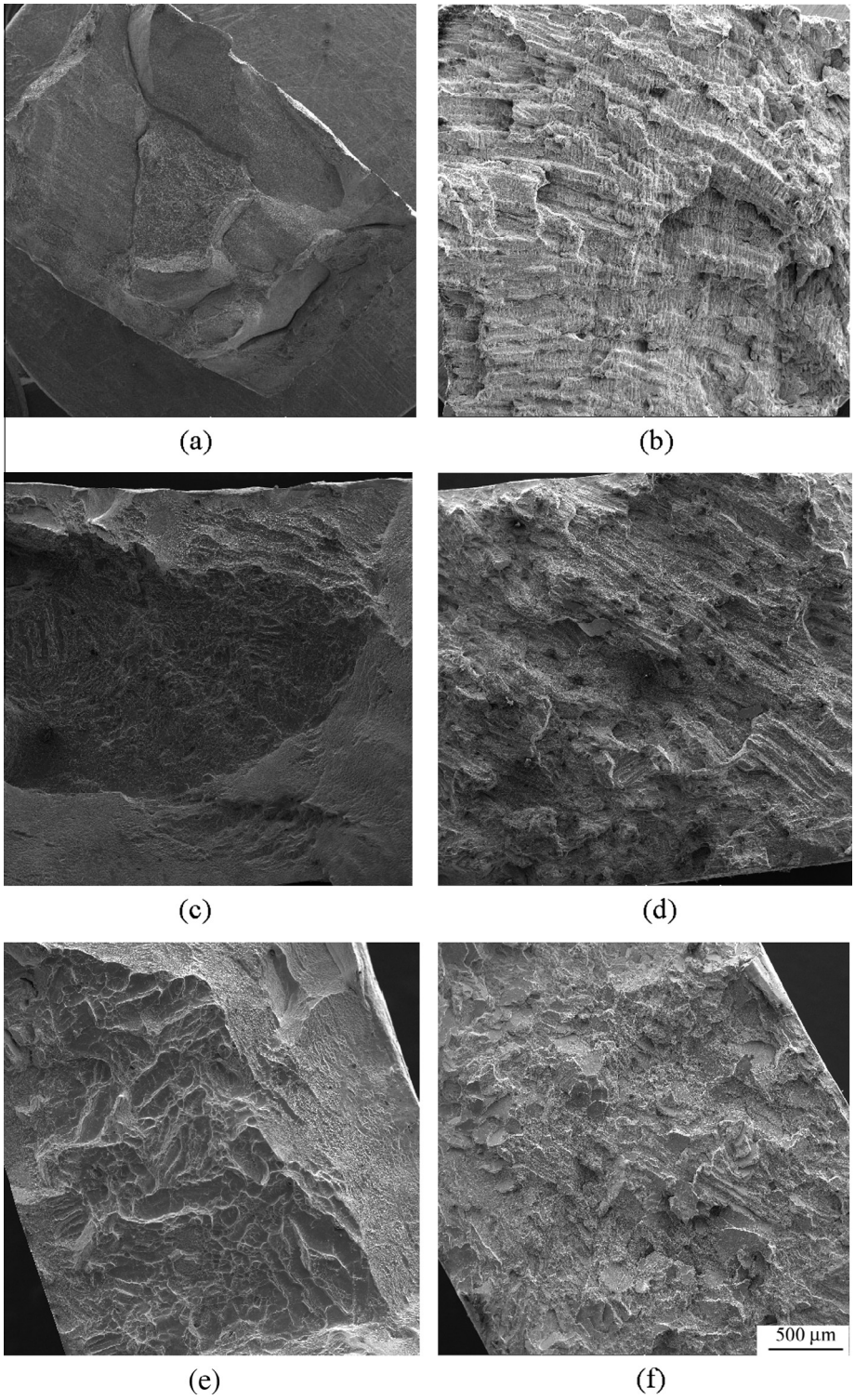

Fig. 12. Fractrographs of solution treated alloys: (a) Ti-15333, (b) Ti-15333BC, (c) Ti-1023, (d) Ti-1023BC, (e) Ti-5553 and (f) Ti-5553BC. The features are finer in boron–carbon containing alloys.

boron–carbon addition may be masked. A slight softening may be due to the scatter in hardness.

Increase in strength values (Table 5) can be attributed again to the refinement in microstructure. As mentioned earlier, because of the presence of fine alpha, the area fraction of α–β interface that provides effective obstacles to dislocation motion is very high. Since the volume faction of alpha varies from 50% to 60% [24], the deformation in the alpha phase will play a key role on the deformation of the overall aggregate. Fig. 16 shows schematics of dislocation configurations for different slip systems in the alpha phase that is for (a) $\langle 11\bar{2}0\rangle$ (0002), (b) $\langle 11\bar{2}0\rangle$ $\{10\bar{1}0\}$ and (c) $\langle 1\bar{2}0\rangle\{10\bar{1}1\}$. In case of (a) that is basal slip, the relevant microstructural parameter for dislocation motion is the width of the lath assuming that the α lath grows perpendicular to the basal plane. For both prismatic (Fig. 16b) and pyramidal slip (Fig. 16c), the relevant microstructural parameters are both the width and length of

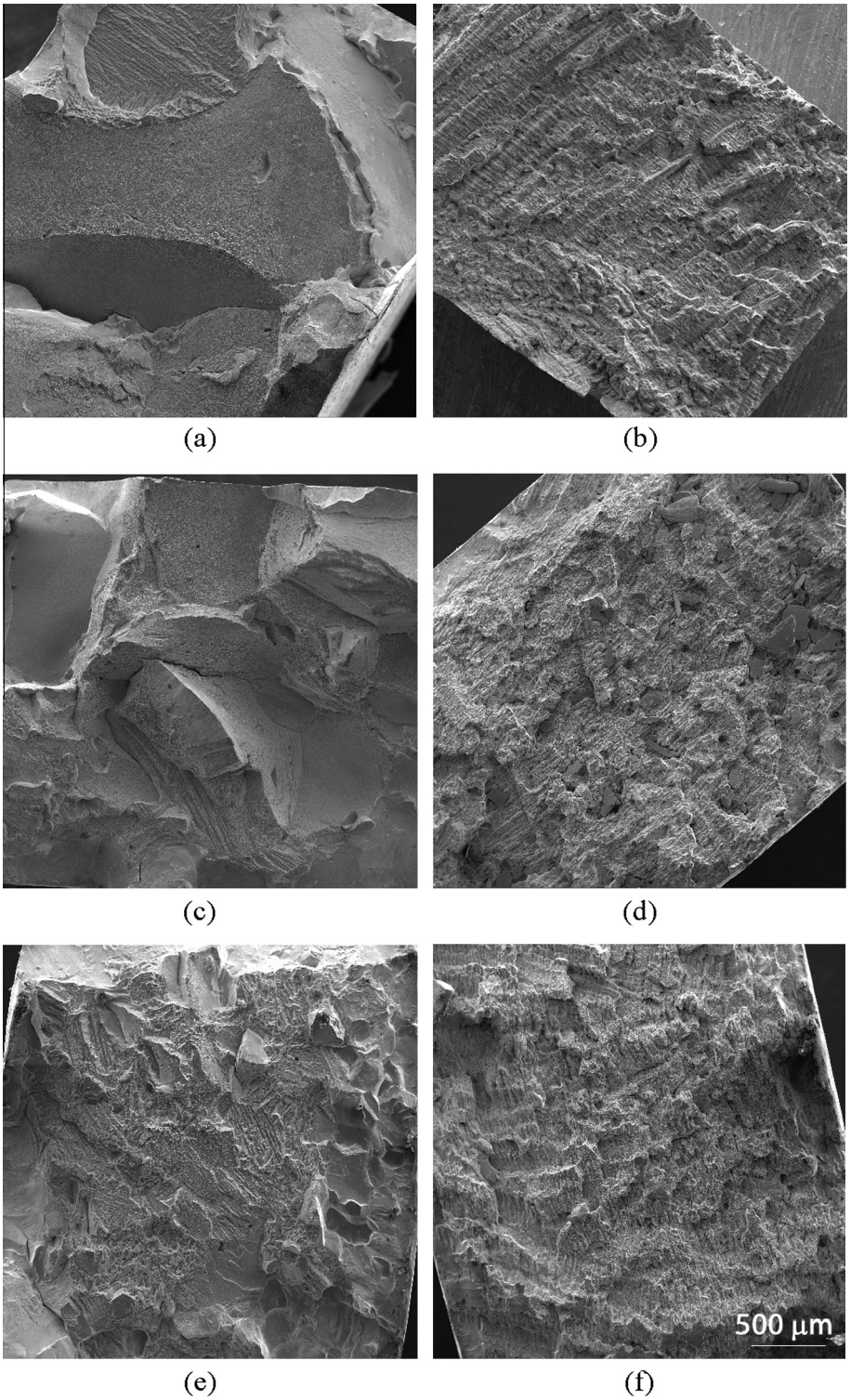

Fig. 13. Fractographs of solution treated plus aged alloys: (a) Ti-15333, (b) Ti-15333BC, (c) Ti-1023, (d) Ti-1023BC, (e) Ti-5553 and (f) Ti-5553BC. The features are finer in B–C containing alloys.

the lath. Strengthening due to Orowan bowing of the dislocation in a precipitate of this size is given by:

$$\sigma = M\mu b/1 \quad (1)$$

where σ is the yield stress, M is Taylor factor (assumed 3.5 in this case) for converting critical resolved shear stress to polycrystalline stress, b = 3.5E−10 m, l = width or length of the α precipitate. Assuming l varies from 50 to 800 nm (Figs. 5 and 8), the estimated strength values for the initiation of macroscopic deformation in the α phase are in the range of 50–1350 MPa, the lower value corresponding to the length and the higher value corresponding to the width of the precipitate. Since it is a two-phase microstructure with volume fraction of β in the range of 40–60%, the plastic flow in β phase will also play a role. The length scale of β phase is similar

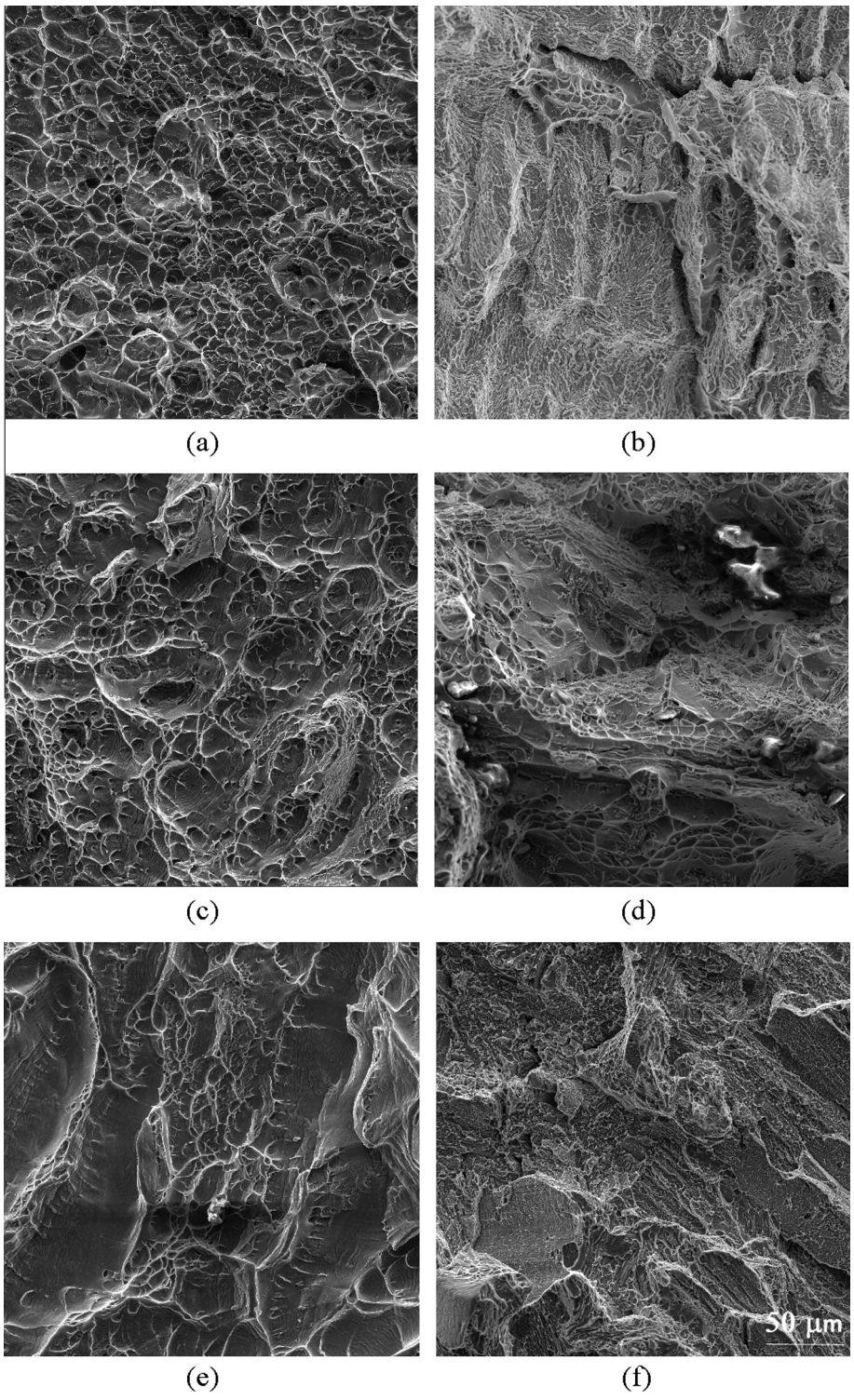

Fig. 14. Fractographs of solution treated alloys: (a) Ti-15333, (b) Ti-15333BC, (c) Ti-1023, (d) Ti-1023BC, (e) Ti-5553 and (f) Ti-5553BC.

to that of alpha which implies that approximately similar strength values are expected if one assumes Orowan looping. The fact that the experimental values of yield strength range from 900 to 1400 MPa indicates the Orowan bowing is able to account for the flow stress values obtained in the aged alloys. Additionally, it appears that the width of alpha lath is a more relevant microstructure parameter as the experimental values are closer to the upper estimate of the proposed mechanism. It is well understood that the actual deformation will be much more complex given the fineness of the aggregate and the range of morphology (from lath to lenticular) exhibited by alpha and also the mean free path provided by retained beta. However, a simplistic approximation involving slip in single phase is at least able to predict the strength value with a reasonable accuracy.

There is substantial decrease in ductility, almost 2–3 times. This is possibly due to the presence of undeformable TiB and TiC particles that tend to crack during plastic deformation. This has been clearly shown in near alpha titanium alloy [16] and metastable beta titanium alloy [10]. Therefore it is felt that more deformation needs to be imparted in the melted ingot so as to refine both the

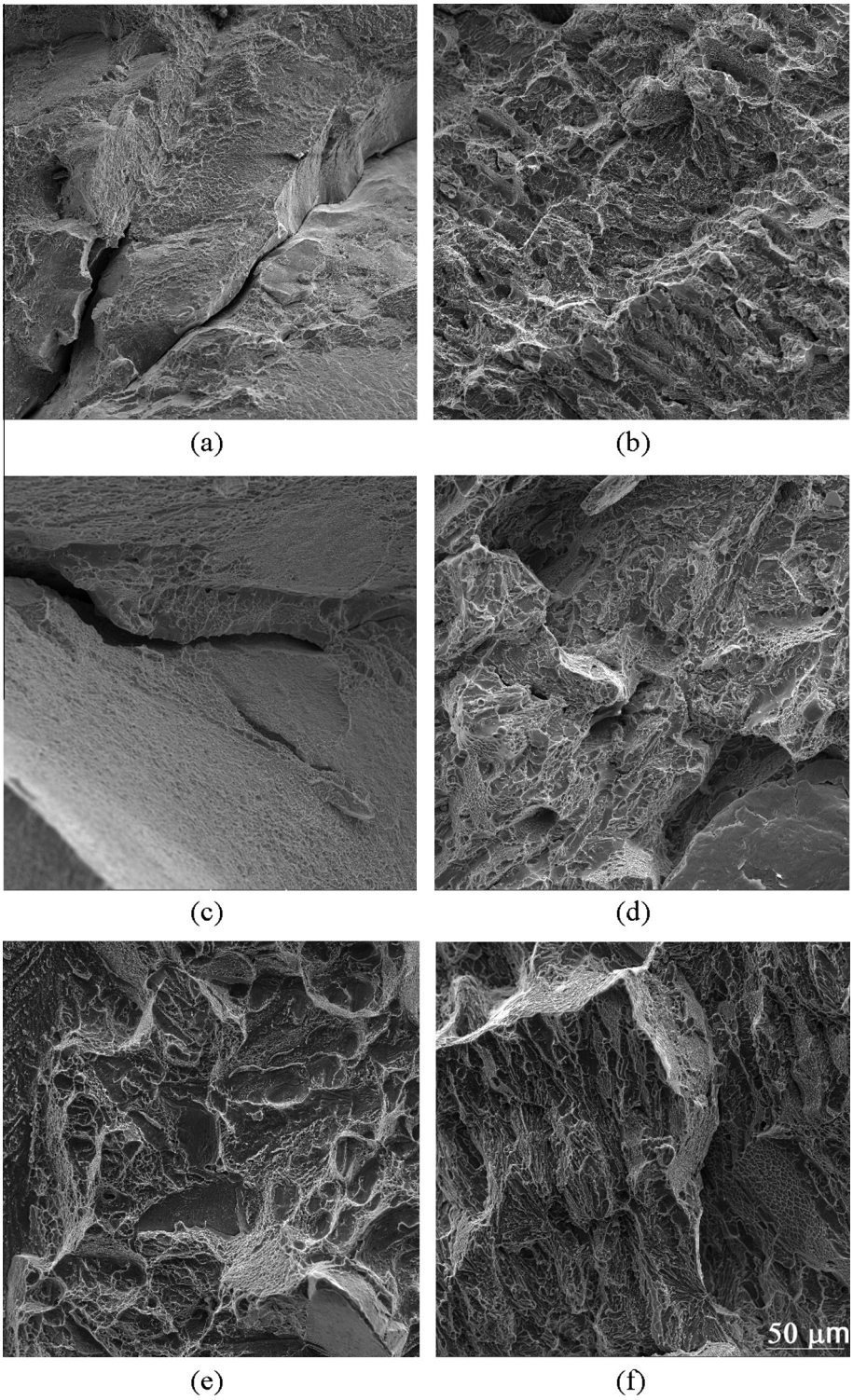

Fig. 15. Fractographs of solution treated plus aged alloys: (a) Ti-15333, (b) Ti-15333BC, (c) Ti-1023, (d) Ti-1023BC, (e) Ti-5553 and (f) Ti-5553BC.

grain structure of the alloy and particle size of borides and carbides. While there is substantial increase in strength values following ageing, significant deterioration of elongation values occurs and a decreasing trend as regards the effect of boron plus carbon does not emerge. This is also consistent with mixed mode failure in the fractograph (Fig. 13) as opposed to transcrystalline dimple failure in the solution treated condition (Fig. 12). Again in this case there is considerable scope for improvement in the properties by optimising the ageing temperature. The very fact that ductile dimples are seen in the aged structure (Fig. 15) points towards plastic deformation at fine scale which can be gainfully utilised by appropriate heat treatment to obtain good macro plasticity.

Fig. 17a shows true stress–true plastic strain of the alloys in solution treatment condition. The alloys Ti-15333, Ti-1023 and Ti-1023BC show conventional double slope behaviour. On the other hand, Ti-15333BC, Ti-5553 and Ti-5553BC show a triple

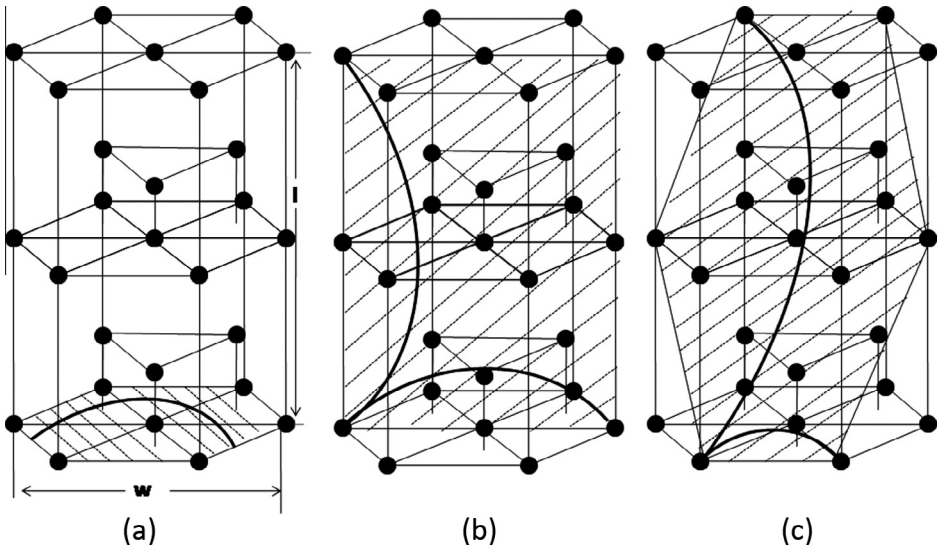

Fig. 16. Schematic of possible dislocation configuration in aged alpha phase.

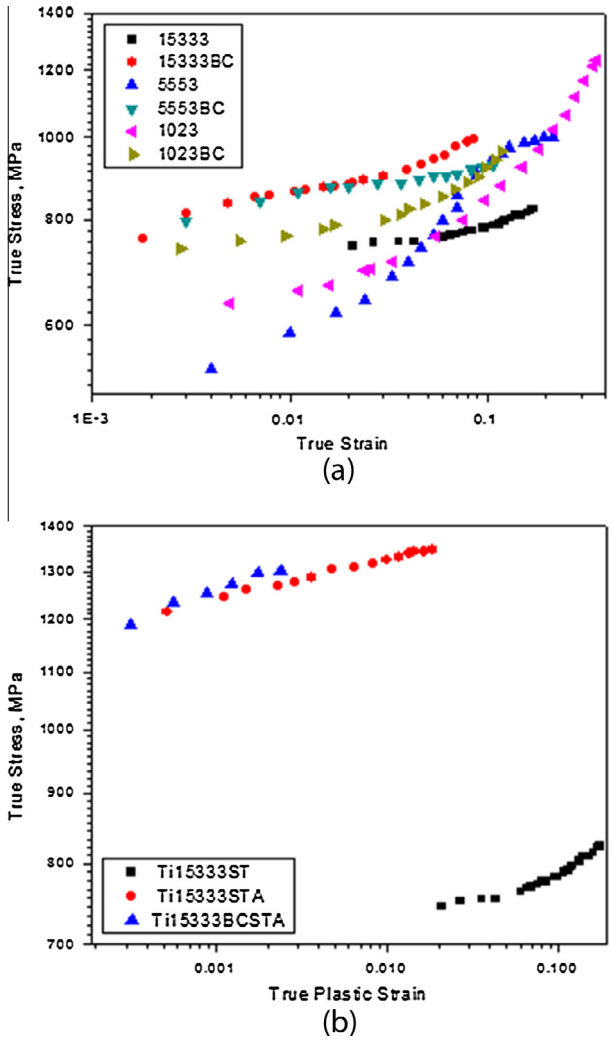

Fig. 17. Log–log plots of true stress versus true strain in (a) solution treatment and (b) solution treatment plus ageing.

slope behaviour. It must be mentioned that the β phase in β-titanium alloys deforms by planar slip [25]. While the lower slope in this plot may be a result of planar slip, the higher slope may be a manifestation of intersecting slip bands and dislocation interactions at higher plastic deformation [26,27]. Since large plastic deformation is obtained in solution treatment condition, the flow mechanisms operative in different plastic deformation regimes may vary, giving rise to diverse work hardening behaviour. A detailed dislocation behaviour using transmission electron microscopy may be needed to understand this.

In order to simplify this behaviour for facilitating comparison, the work/strain hardening exponents (n) calculated for the three alloys and their boron – carbon modification, assuming a single slope behaviour in the plastic regime of their tensile stress–strain curves, are given in Table 6. This table shows that amongst the three base alloys, Ti-5553 has the highest value of work hardening exponent followed by Ti-1023. The boron plus carbon modification leads to decrease in the work hardening exponent except in the case of Ti-15333, where it leads to an increase of about 0.010. The beta titanium alloys normally have low values of 'n', because of predominantly planar slip due to ω phase formation [25]. As the amount of Al content increases, it destabilises ω phase and decreases the tendency for planar slip behaviour resulting in a more uniformly distributed dislocation tangles. This leads to the increase in work hardening and gets reflected in higher 'n' values. Similar behaviour is clearly observed in case of Ti-5553 with 5 wt.% Al (highest amongst all the alloys investigated in the present study). The alloy Ti-1023 forms stress induced martensite in beta solution treated condition and that also leads to a comparatively higher values of 'n' in the present study.

In solution treatment plus aged condition (Fig. 17b), single slope behaviour is clearly seen. It is to be noted that the plastic deformation is considerably low here. The data points corresponding to boron–carbon alloy overlap with those of the base alloy thereby suggesting that the effect due to the addition of these elements on the work hardening behaviour is not significant.

Table 6
Work/strain hardening exponent (n), calculated for different alloys, assuming a single slope behaviour in the plastic regime.

Alloy	n
Ti-15333	0.05
Ti-15333BC	0.06
Ti-5553	0.18
Ti-5553BC	0.04
Ti-1023	0.16

5. Conclusions

A detailed study on the effect of boron and carbon addition on microstructure and mechanical properties of different β-titanium alloys in two heat treatment conditions: (i) solution treatment and (ii) solution heat treatment plus aging has been carried out. The salient conclusions are as follows:

(1) Addition of boron and carbon results in refinement of β grain size. It also leads to refinement in the size of aged α after ageing.
(2) Hardness and tensile strength increase with the addition of boron and carbon in solution heat treatment condition. This is due to the presence of undeformable boride and carbide particles and also refinement in grain size.
(3) There is substantial decrease in ductility in boron and carbon containing alloys in solution treatment condition, which is due to the presence of brittle carbide and boride particles.
(4) Upon ageing, there is an increase in strength and hardness and decrease in ductility, which in attributed to the precipitation of α. In this case, the strengthening due to boron and carbon is marginal. The loss in ductility is again due to the presence of fine alpha which makes deformation difficult.
(5) While multiple slopes in work hardening plots, in solution treatment conditions, indicate different flow mechanism, the aged alloys show a single behaviour pointing towards a single flow mechanism. The presence of aluminium leads to increase in overall work hardening.

Acknowledgements

Authors convey their sincere gratitude to Dr. Amol A. Gokhale, Outstanding Scientist & Director, DMRL, India for encouragement and kind permission to publish this work. They would also like to thank Dr. T. Srinivas Rao, Director, NIT, Warangal, India for his encouragement and advice.

References

[1] Boyer RR. Applications of beta titanium alloys in airframes. In: Eylon D, Boyer RR, Koss DA, editors. Beta titanium alloys in the 1990's. Pennsylvania: TMS; 1993. p. 335–46.
[2] Boyer RR. An overview on the use of titanium in the aerospace industry. Mater Sci Eng A 1996;213:103–14.
[3] Boyer RR, Briggs RD. The use of β titanium alloys in the aerospace industry. J Mater Eng Perform 2005;14(6):681–5.
[4] Bania PJ. Beta titanium alloys and their role in the titanium industry. In: Eylon D, Boyer RR, Koss DA, editors. Beta titanium alloys in the 1990's. Pennsylvania: TMS; 1993. p. 3–14.
[5] Srinivasu G, Natraj Y, Bhattacharjee A, Nandy TK, Nageswara Rao GVS. Tensile and fracture toughness of high strength β Titanium alloy, Ti–10V–2Fe–3Al, as a function of rolling and solution treatment temperatures. J Mater Des 2013;47:323–30.
[6] Chen ZQ, Hu D, Loretto MH, Wu X. Influence of 0.2 wt-%C on the aging response of Ti-15-3. Mater Sci Technol 2004;20:756–64.
[7] Bermingham MJ, McDonald SD, Nogita K, St John DH, Dargush MS. Effects of boron on microstructure in cast titanium alloys. Scr Mater 2008;59:538–41.
[8] Tamirisakandala S, Bhat RB, Tiley JS, Miracle DB. Grain refinement of cast titanium alloys via trace boron addition. Scr Mater 2005;53:1421–6.
[9] Cherukuri B, Srinivasan R, Tamirisakandala S, Miracle DB. The influence of trace boron addition on grain growth kinetics of the beta phase in the beta titanium alloy Ti-15Mo-2.6Nb-3Al-0.2Si. Scr Mater 2009;60:496–9.
[10] Sarkar R, Ghosal P, Muraleedharan K, Nandy TK, Ray KK. Effect of boron and carbon addition on microstructure and mechanical properties of Ti-15-3 alloy. Mater Sci Eng A 2011;528:4819–29.
[11] Tamirisakandala S, Bhat RB, Tiley JS, Miracle DB. Grain refinement of cast titanium alloys via trace boron addition. J Mater Eng Perform 2005;14:741–6.
[12] Tamirisakandala S, Miracle DB, Srinivasan R, Gunasekera JS. Titanium alloyed with boron. Adv Mater Proc 2006;164(12):41–3.
[13] Ranganath S, Mishra RS. Steady state creep behaviour of particulate-reinforced titanium matrix composites. Acta Mater 1996;44:927–35.
[14] Boyer R, Welsch G, Collings EW, editors. Materials properties handbook: titanium alloys. Materials Park, OH: ASM International; 1994. p. 439–46.
[15] Fanning JC, Boyer RR. A near beta titanium alloy for airframe application. In: Lutjering G, Albrecht J, editors. Ti-Sc. and Tech., 4. Verlag-VCH; 2003. p. 2643–50.
[16] Chandravanshi VK, Sarkar R, Ghosal P, Kamat SV, Nandy TK. Effect of minor additions of boron on microstructure and mechanical properties of as-cast near titanium alloy. Metall Mater Trans A 2010;41:936–46.
[17] Sen I, Tamirisakandala S, Miracle DB, Ramamurthy U. Microstructural effects on the mechanical behaviour of boron-modified Ti-6Al-4V alloys. Acta Mater 2007;55:4983–93.
[18] Wu X, del Prado J, Li Q, Huang A, Hu D, Loretto MH. Analytical electron microscopy of C-free and C-containing Ti-15-3. Acta Mater 2006;54:5433–48.
[19] Sarkar R, Ghosal P, Nandy TK, Ray KK. Structure–property correlation of a boron and carbon modified as cast β titanium alloy. Philos Mag 2013;93:1936–57.
[20] Hall EO. The deformation and ageing of mild steel: III discussion of results. Proc Phys Soc London B 1951;64:747.
[21] Petch NJ. The cleavage strength of polycrystals. J Iron Steel Inst 1953;174:25–8.
[22] Boehlert CJ, Tamirisakandala S, Curtin WA, Miracle DB. Assessment of in situ TiB whisker tensile strength and optimization of TiB-reinforced titanium alloy design. Scr Mater 2009;61:245–8.
[23] Chandravanshi VK, Sarkar R, Kamat SV, Nandy TK. Effect of boron on microstructure and mechanical properties of thermo mechanically processed near alpha titanium alloy Ti-1100. J Alloys Compd 2011;5(09):5506–14.
[24] Sarkar R. Effect of aged microstructures on the strength and work hardening behaviour of Ti-15V-3Cr-3Sn-3Al, in preparation, DMRL.
[25] Bhattacharjee A, Ghosal P, Gogia AK, Bhargava S, Kamat SV. Room temperature plastic flow behaviour of Ti-6.8Mo-4.5Fe-1.5Al and Ti-10V-4.5Fe-1.5Al: effect of grain size and strain rate. Mater Sci Eng A 2007;452–453:219–27.
[26] Banumathy S, Mandal RK, Singh AK. Hot rolling of binary Ti-Nb alloys Part II: mechanical properties anisotropy. Int J Mater Res 2011;102(2):208–17.
[27] Choudhary BK, Samuel EI, Bhanu Sankara Rao K, Mannan SL. Tensile stress–strain and work hardening behaviour of 316LN austenitic stainless steel. Mater Sci Technol 2001;17(2):223–31.